Plasmonic films with a periodic arrangement of sub-wavelength slits

Peter B. Catrysse*, Georgios Veronis, Jung-Tsung Shen, Hocheol Shin, and Shanhui Fan
Edward L. Ginzton Laboratory, Stanford University, Stanford, CA 94305

ABSTRACT

In a recent paper [Phys. Rev. Lett. **94**, 197401 (2005)], we introduced a mechanism for creating artificial high refractive index metamaterials by exploiting the existence of sub-wavelength propagating modes in metallic systems. We showed that a perfect metal film with a periodic arrangement of sub-wavelength cut-through slits can be regarded as a dielectric slab with a frequency-independent effective index. Here, we discuss the optical properties of such a system when the perfect metal condition is no longer valid, e.g., in the visible and near infrared wavelength regimes. If the metal obeys a plasmonic dispersion model, we find that films with a periodic arrangement of sub-wavelength slits support two distinct types of guided modes: a surface mode and a set of effective dielectric slab modes. We show how the behavior of both modes is affected by film thickness and surface properties.

Keywords: metamaterials, thin metal film, waveguide, plasmonic dispersion, sub-wavelength slits

1. INTRODUCTION

Recently, there has been great interest in exploiting sub-wavelength resonances in metallic structures to create artificial materials with unusual effective electromagnetic responses. Notable examples include high-impedance surfaces used as an antenna substrate,[1] negative refractive index metamaterials,[2,3] effective surface plasmon behavior on perfect metal surface with gratings,[4] and effective bulk plasmon behavior in thin-wire structures.[5,6] In a recent paper,[7] we introduced a mechanism for creating artificial high refractive index metamaterials by exploiting the existence of sub-wavelength propagating modes in metallic systems. We showed that a perfect metal film with a periodic arrangement of cut-through slits can be regarded as a dielectric slab with a frequency-independent effective refractive index. The effective index in this system is entirely controlled by geometry, and indices that are arbitrarily high can be straightforwardly synthesized. Such a capability is potentially important for miniaturization of optical or electromagnetic devices and for improving resolution in imaging. More fundamentally, the refractive index is commonly regarded as an intrinsic material property that is directly related to the underlying electronic states. By pointing out that the refractive index can be controlled by geometry only, we added evidence to the important potential of replacing electronic states with sub-wavelength electromagnetic resonances. This in turn could open up a new world of possibilities in optical physics. In this paper, we summarize the results obtained for perfect metal films and we analyze the optical properties of such a system when the perfect metal condition is no longer valid, e.g., in the visible and near infrared wavelength regimes.

2. METAMATERIALS BASED ON PERFECT METAL FILMS

The key to creating the desired effective index behavior lies in the existence of sub-wavelength propagating modes in metallic structures. As an example, we consider a perfect metal film with one-dimensional periodic cut-through slits, as shown in Fig. 1(a). Without losing generality, we assume hereafter vacuum for the ambient environment and the slit regions. In the slits, regardless of how small the width is, there always exists a propagating transverse electromagnetic (TEM) mode, with the electric field pointing in the x direction. It has been shown[8-10] that the presence of this mode permits perfect transmission of light through sub-wavelength slit arrays. Here, in order to define an appropriate effective index, we focus on the behavior of this structure in the long-wavelength limit. As it turns out, the properties of the metal film for the transverse magnetic (TM) polarization asymptotically approach those of a dielectric slab with a uniquely defined refractive index n and a width $\overline{L}$, as depicted in Fig. 1(b).

* Email: pcatryss@stanford.edu, Phone: (650) 736-2309, Web: www.stanford.edu/~pcatryss

Photonic Crystal Materials and Devices IV, edited by Ali Adibi, Shawn-Yu Lin, Axel Scherer,
Proc. of SPIE Vol. 6128, 612818, (2006) · 0277-786X/06/$15 · doi: 10.1117/12.648510

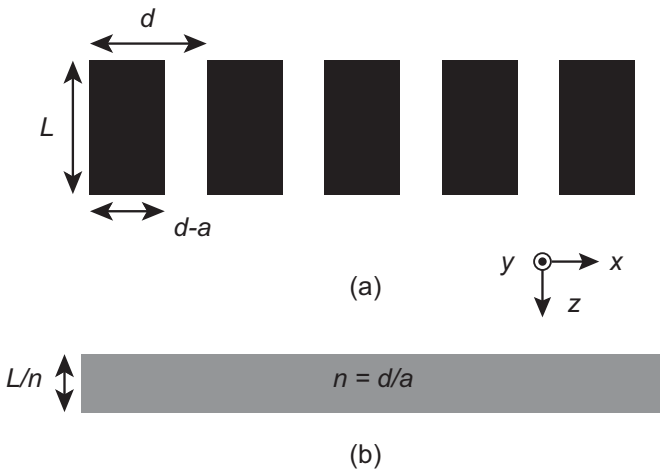

Figure 1: (a) Schematic of a metal film with periodic cut-through slits. The parameters are defined as in the figure: a is the width of the slit, d is the periodicity, and L is the thickness of the metal film. The black regions indicate metal parts and the white regions correspond to vacuum. The film is extended in the x-y plane. (b) The equivalent effective dielectric slab corresponding to (a). The effective refractive index is $n \equiv d/a$, and the thickness is $\bar{L} \equiv L/n$.

1. Heuristic derivation

We first give a heuristic derivation to establish the connection between the metal film and the dielectric slab. Our heuristics are based on fundamental concepts such as resonance, instantaneous power flow, and energy conservation. Specifically, the Fabry-Perot resonance condition for the TEM mode in the slit is $k \times L \approx m\pi$, where $k = 2\pi/\lambda$ is the wave vector of the incident light, L is the thickness of the metal film, and m is a positive integer. This condition can be written as $(nk)\times(L/n) \approx m\pi$, which implies that any dielectric slab with refractive index n and thickness $\bar{L} \equiv L/n$ would give the same Fabry-Perot resonances. To uniquely determine the refractive index, we compare the fields in both systems. We will use an overhead line over a variable to denote the corresponding quantity in the effective medium. Suppose that the effective homogeneous electric field in the effective medium is $\bar{\mathbf{E}}$; we then have $\bar{\mathbf{E}} = a/d\ \mathbf{E}$. Requiring the instantaneous energy flow across the surface to be the same for both the metal film and the effective dielectric slab, $(\mathbf{E}\times\mathbf{H})_z\, a = (\bar{\mathbf{E}}\times\bar{\mathbf{H}})_z\, d$, we obtain the scaling condition for the magnetic fields $\bar{\mathbf{H}} = \mathbf{H}$. Note that, for the TEM mode considered here, the only nonzero fields are E_x and H_y. In addition, Maxwell's equations give the following relations between the electric and magnetic fields: $\bar{\mathbf{E}}/\bar{\mathbf{H}} = \sqrt{\bar{\mu}/\bar{\varepsilon}}$ and $\mathbf{E}/\mathbf{H} = \sqrt{\mu/\varepsilon}$. By imposing the condition that the total energy for both systems is the same,

$$\frac{1}{2}\left(\varepsilon\mathbf{E}^2 + \mu\mathbf{H}^2\right) L\, a = \frac{1}{2}\left(\bar{\varepsilon}\bar{\mathbf{E}}^2 + \bar{\mu}\bar{\mathbf{H}}^2\right)_z \bar{L}\, d \tag{1}$$

we have $\bar{\mu} = \mu$ and $\bar{\varepsilon}/\varepsilon = (d/a)^2$, and therefore the effective refractive index is $n \equiv d/a$. Consequently, it seems possible to synthesize an effective refractive index entirely by geometrical means. This would allow the creation of arbitrary large frequency-independent refractive indices without changing the intrinsic electronic states of a material.

2. Rigorous calculation

We now confirm this intuitive argument by performing rigorous calculations of the optical properties of the metal film and the dielectric slab. Consider a TM wave (magnetic fields pointing in the y direction) incident on the metal film.

2.1. Transmission

The transmission amplitude for the p-th diffraction order is given by[8-10]

$$t_p = \frac{\omega/c}{\alpha_p} g_p \left(\frac{4fu}{(1+\phi)^2 - (1-\phi)^2 u^2} \right), \tag{2}$$

where ω is the frequency, c is the speed of light, $G_p = k_x + 2\pi p/d$ is the parallel quasi-momentum along the metal surface of the p-th diffraction order, $\alpha_p = \sqrt{(\omega/c)^2 - G_p^2}$ is the momentum in the z direction, $f = a/d$ is the area filling factor of the slits, $u = \exp(i\omega/c\, L)$ is the phase accumulation across the metal film with thickness L, $g_p = \mathrm{sinc}(G_p\, a/2)$, and

$$\phi = \sum_{p=-\infty}^{\infty} f g_p^2 \frac{\omega/c}{\alpha_p}. \tag{3}$$

At normal incidence, $g_0 = 1$ and $\alpha_0 = \omega/c$. The zero-th order amplitude, which is the amplitude of the only field that propagates afar when the wavelength λ is larger than the periodicity d, can be written as

$$t_0 = \frac{4\left[\left(f/\phi^2 \right) / \left(1+1/\phi \right)^2 \right] e^{i(\omega/c)L}}{1 - \left[\left(1-1/\phi \right) / \left(1+1/\phi \right) \right]^2 e^{i2(\omega/c)L}}. \tag{4}$$

Comparing this to the transmission amplitude of a plane wave normally incident on a dielectric slab with refractive index n and thickness $\bar{L}$,

$$t_0 = \frac{4\left[n/\left(1+n \right)^2 \right] e^{in(\omega/c)\bar{L}}}{1 - \left[\left(1-n \right) / \left(1+n \right) \right]^2 e^{i2n(\omega/c)\bar{L}}}, \tag{5}$$

it follows immediately, by identifying $n = 1/\phi$ and $\bar{L} = L/n$, that these two amplitudes are asymptotically identical. Note that, in this case $1/\phi \approx 1/f = d/a$, while higher diffraction orders introduce a small purely imaginary correction. It is easy to show that the identification becomes very accurate for a large d/a ratio, i.e., high effective refractive index n. This confirms the notion of the corresponding "effective dielectric slab" given earlier by the heuristic argument: the transmission properties of a metal film with slits are asymptotically identical to those of a dielectric slab with the refractive index $n \equiv d/a$ and the thickness $\bar{L} \equiv L/n$. The identification to the dielectric slab remains valid for oblique incidence as well.

The transmission spectrum for normally incident light is shown in Fig. 2(a) for the case $n = 4$. The spectrum is calculated using the exact analytic expression Eq. (4). The transmission coefficient becomes 100% when $k \times L = \omega/c \times L \approx m\pi$, as expected from the Fabry-Perot resonance condition in the slit. Remarkably, the entire spectrum matches almost exactly that of a high index slab with $n \equiv d/a$ and $\bar{L} \equiv L/n$. Actually, it can be made to match by scaling the thickness $\bar{L}$ by a few percent. For obliquely incidence, the transmission spectrum is shown in Fig. 2(b) as a function of the angle θ.

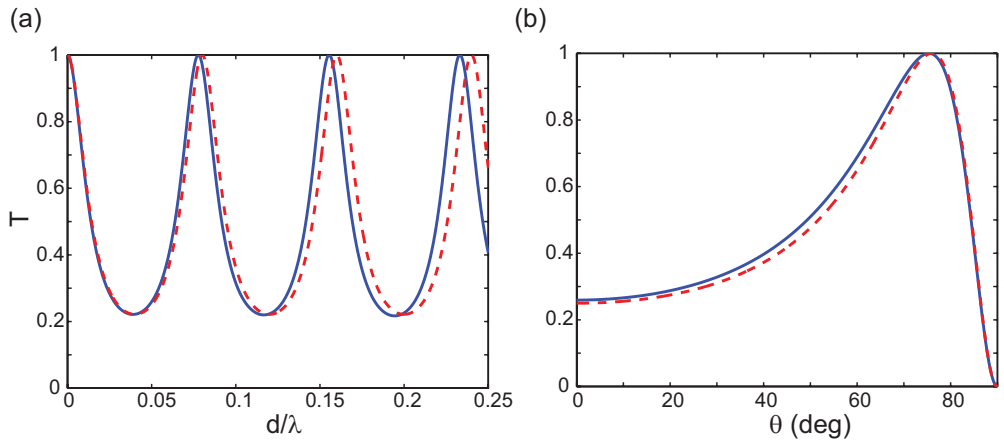

Figure 2: (Color online) The transmission coefficient of the metal film (solid blue lines) and the corresponding effective dielectric slab (dashed red lines). The thickness of the metal film is $L/d = 25/4$. The effective refractive index of the slab is $n = d/a = 4$. (a) Transmission spectrum at normal incidence ($\theta = 0$). (b) Transmission at oblique incidence for the frequency $\omega = 0.05\, d/\lambda$.

2.2. Waveguiding

With the transmission equivalence established, it would be of great interest if the notion of the effective dielectric slab could be carried over to other optical properties, such as wave-guiding along the medium. As noted by the expression for α_p, i.e., the momentum of the p-th diffraction order field external to the metal film in the z direction, when the periodicity of the slits is much smaller than the free-space wavelength of light, all diffraction orders are evanescent in the z direction.

These diffraction orders form sizable high intensity bulges centered on the openings of the slits.[8] When these bulges overlap with each other and create propagating modes in the structure, the metal film could act as a waveguide. Recently, it has been shown that structured surfaces on perfect metal can support surface modes that are evanescent inside the structures.[4] In contrast, in our system, due to the propagating nature of the TEM modes in the slits, the guided modes are not surface states but rather closely resemble waveguide modes in a dielectric slab.

The properties of such guided modes can be solved for analytically. When there is no external source present, the magnetic fields in the m-th slit, above the metal film and below the metal film, have the following forms:

$$
\begin{aligned}
H_y^m(x,z) &= \left[A^m(x)\cos\left(\frac{\omega}{c}z\right) + B^m(x)\sin\left(\frac{\omega}{c}z\right)\right] \quad for\,|x-md| \le \frac{a}{2}, \\
H_y^{above}(x,z) &= e^{ik_x x}\sum_{p=-\infty}^{\infty} r_p e^{i\alpha_p(-z-L/2)} e^{i(2\pi p/d)x}, \\
H_y^{above}(x,z) &= e^{ik_x x}\sum_{p=-\infty}^{\infty} t_p e^{i\alpha_p(z-L/2)} e^{i(2\pi p/d)x},
\end{aligned}
\tag{6}
$$

respectively; A^m, B^m, r_p, and t_p are the amplitudes. The electric fields are then obtained from $\varepsilon\,\partial\mathbf{E}/\partial t = \nabla\times\mathbf{H}$. The even eigenmodes ($r_p = t_p$ for all p, and $B^m = 0$ for all m) satisfy the dispersion relation

$$
\frac{1}{i\phi} = \tan\left(\frac{\omega}{c}\frac{L}{2}\right) \tag{7}
$$

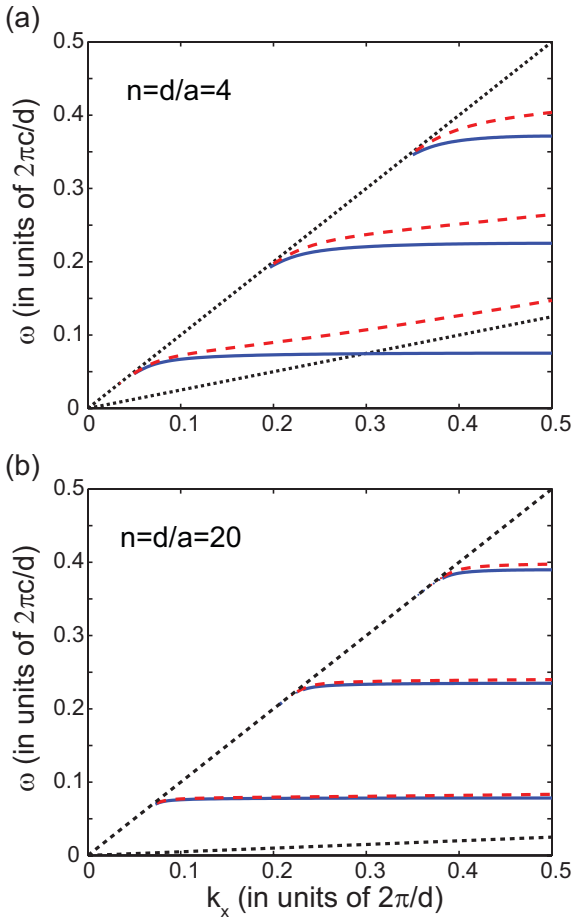

Figure 3: (Color online) Dispersion curves of the waveguide modes in the first Brillouin zone. Shown in the figures are the first three even modes of the metal film (solid blue lines) and the corresponding effective dielectric slab (dashed red lines). The dotted black lines are the light lines in vacuum and in the slab waveguides, respectively. The thickness of the metal film is $L/d = 25/4$. The effective refractive index of the slab is (a) $n = d/a = 4$ and (b) $n = 20$. (The odd modes, not shown here, are located between the even bands and behave similarly.)

and the odd eigenmodes ($r_p = -t_p$ for all p, and $A^m = 0$ for all m) satisfy the dispersion relation

$$\frac{1}{i\phi} = -\cot\left(\frac{\omega}{c}\frac{L}{2}\right) \tag{8}$$

as calculated by matching the boundary conditions.[8,9] In both cases, $\phi = \sum_{p=-\infty}^{\infty} f g_p^2 (\omega/c)/\alpha_p$ as defined in Eq. (3), is now purely imaginary for waveguide modes. When we compare Eqs. (7) and (8) with the corresponding dispersion relations of the TM modes of a dielectric slab with refractive index n and thickness $\bar{L} = L/n$, the mapping $n = 1/\left(f g_0^2\right)$ becomes asymptotically exact for large n. In practice, $k_x a \ll 1$, so $g_0 = \mathrm{sinc}\left(k_x a/2\right) \approx 1$ and therefore $n \approx 1/f = d/a$, which is the same condition as for transmission. Figure 3 shows the dispersion curves of the first three even waveguide modes in the first Brillouin zone of two metal films ($d/a = 4$ and 20, respectively) and the corresponding effective dielectric slabs.

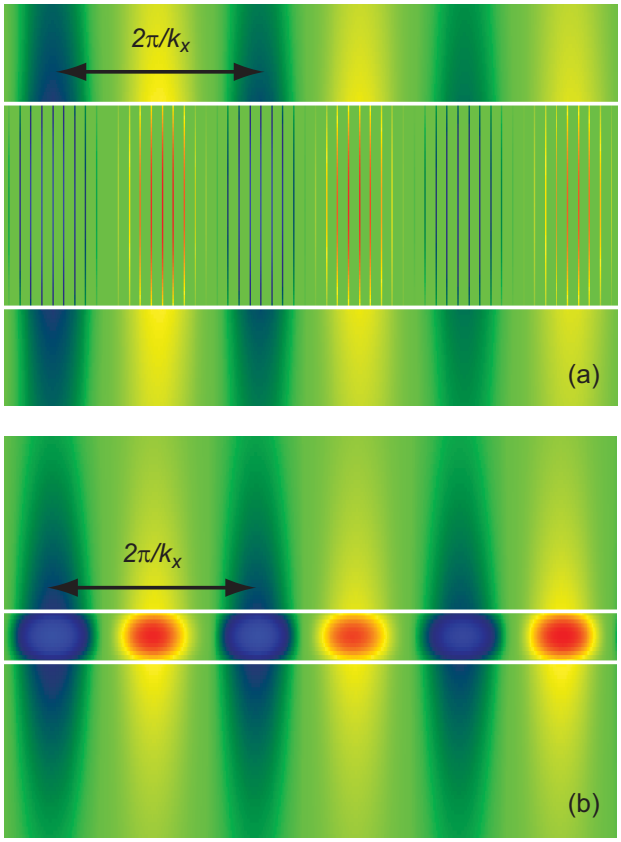

Figure 4: (Color online) Snapshots of the H_y field distributions of the fundamental waveguide modes of the metal film [shown in (a)] and the corresponding effective dielectric slab [shown in (b)] for $n = d/a = 4$, $L/d = 25/4$. The red color indicates positive amplitude, while the blue color indicates negative amplitude. The white lines in (a) and (b) outline the film and the slab, respectively. The normalized excitation frequency is $\omega = d/\lambda = 0.0516$. The arrows indicate the periodicity of the field.

At low frequency, the wave propagates at the speed of light in the external region, while at large propagating constant k_x, the eigenfrequencies approach $(2p-1)\pi c/L$ (for even modes) and $2p\pi c/L$ (for odd modes), respectively, where p is a positive integer. The even and odd modes stack up alternatively and are equally spaced at large k_x. As expected, the agreement between the metallic system and the effective dielectric slab improves as n increases.

For $n = 20$, the two dispersion curves almost completely overlap within the first Brillouin zone. Both the transmission and the waveguide properties of the metal film give the same expression for the effective refractive index $n = d/a$, thereby validating the generality of the effective refractive index.

Figure 4 shows the modal patterns of the fundamental waveguide modes of a metal film and the corresponding effective dielectric slab with the refractive index $n = 4$. These field distributions are computed using a two-dimensional finite-difference time-domain method. The normalized excitation frequency $\omega = d/\lambda = 0.0516$ is in the overlap region of the two dispersion curves in Fig. 3(a). The spatial periodicity of the waveguide modes clearly demonstrates the equivalence of the two systems. The fundamental mode in the metallic structure peaks at the center just as the corresponding guided mode in the dielectric slab does, and this distinctly differs from the surface mode behaviors considered in previous work.[4]

3. Discussion

For transverse-electric (TE) polarization (electric field pointing in the y direction), the slits support only evanescent modes. An similar argument as in Ref. 6 gives $\bar{\mu}_x / \mu_x = 8/\pi^2\, a/d$ and a dielectric function of the plasma form

$$\frac{\bar{\varepsilon}_y}{\varepsilon_y} = \frac{\pi^2}{8}\frac{d}{a}\left(1 - \frac{\omega_p^2}{\omega^2}\right), \tag{9}$$

where the geometrical plasma frequency $\omega_p \equiv \pi c / \left(a\sqrt{\varepsilon_y \mu_x}\right)$; ε_y and μ_x are the dielectric constant and permeability, respectively, of any material that may be filling the slits. The limiting wavelength λ_g for this polarization is $2a$. Since the structure considered here is two-dimensional, its behavior is strongly polarization dependent. The mechanism of creating effective high refractive index dielectric structures is not restricted to two dimensions.

3. PLASMONIC FILMS WITH SUB-WAVELENGTH SLITS

The results presented in the previous section can be directly applied in the wavelength range from microwave to far infrared, where the loss and the plasmonic effects of metals can be largely neglected. In the optical wavelength range, the presence of the plasmonic response leads to additional sub-wavelength propagating modes.[11-13] If the metal obeys a plasmonic dispersion model, we find in the long wavelength regime that the system shown in Fig. 1(a) (see also inset of Fig. 5) supports two distinct types of TM guided modes (magnetic fields parallel to the slits (H_y)) propagating in a direction perpendicular to the slits. The first type is a well-known *surface mode*. This mode is confined to the front and back metal-dielectric interfaces of the film. As in the perfect metal case, the second type originates from sub-wavelength electromagnetic states supported by the slits. In slits, regardless of how narrow they are, there always exists a propagating state. In the transmission regime, this state enables enhanced transmission.[8,10,14] In the guided regime, it gives rise to guided modes, which closely resemble waveguide modes in a dielectric slab. We refer to them as effective *dielectric slab modes*.

1. Methods and models

We calculate the dispersion relations of both types of guided modes using a finite-difference frequency-domain method. Specifically, we solve the wave equation for H_y (E_y) in the case of TM (TE) polarization.[15,16] The computational domain consists of a single period of the structure with the following boundary condition at the left and right boundaries[17]

$$\phi(x+d) = \exp(ik_x d)\phi(x), \tag{10}$$

where d is the periodicity of the structure and $\phi = H_y$ (E_y) for TM (TE) polarization. Perfectly matched layer (PML) absorbing boundary conditions are used at the top and bottom boundaries.[18] We excite a point source and find the eigenfrequencies as discrete peaks in the detected frequency spectrum. We describe the optical properties of the metal using a Drude free-electron model:

$$\varepsilon_2(\omega) = 1 - \frac{\omega_p^2}{\omega\left(\omega - i\omega_\tau\right)}, \tag{11}$$

where ω_p is the plasma frequency and ω_τ is the collision frequency. This dielectric function takes into account the contribution of free electrons only. We refer to it as the *plasmonic model*. Despite its apparent simplicity, the plasmonic model has been the source of valuable insights into the general behavior of real metals.

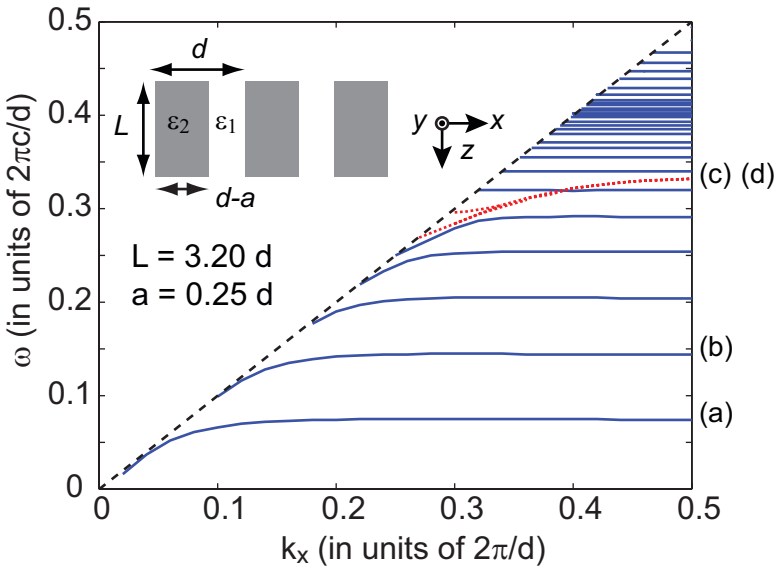

Figure 5: (Color online) Guided-mode band diagram for TM polarization in the first Brillouin zone for $L = 128\,nm$, $d = 80\,nm$, $a = 20\,nm$. Shown are two degenerate surface modes (dotted red curves) and a series of effective dielectric slab modes (solid blue curves). The dashed line is the light line in vacuum. Inset shows the schematic of a metallic film with periodic slits. The gray regions indicate metal (ε_2) and the white regions represent vacuum ($\varepsilon_1 = 1$).

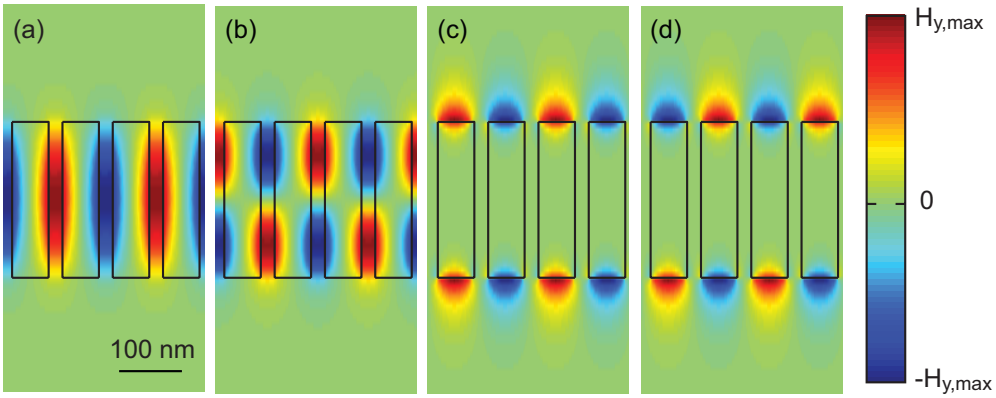

Figure 6: (Color online) H_y-field distributions for the two types of guided modes supported by the geometry shown in Fig. 5. Distributions are shown for $k_x = 0.50$ in units of $2\pi/d$. Frequencies are given in units of $2\pi c/d$. (a) Fundamental effective dielectric slab mode at $\omega = 0.074$, (b) next-higher-order effective dielectric slab mode at $\omega = 0.144$, and (c) and (d) surface modes at $\omega = 0.332$. Red and blue correspond to large positive and negative field values, respectively, and green represents zero field.

In the guided band diagram calculations presented here, we assume a lossless plasmonic model in which we neglect absorption by setting the collision frequency to zero, $\omega_\tau = 0$. It was found from previous band diagram calculations of metallic photonic crystals, in which a plasmonic model was used, that the real part of the band structure is hardly affected by absorption for realistic amounts of absorption.[19] We use $\omega_p = 1.36884 \times 10^{16}\ rad/s$, which is representative of metals (e.g., silver). Without loss of generality, we also assume hereafter vacuum for the ambient dielectric environment and the slit regions, i.e., $\varepsilon_1 = 1$.

2. Results and discussion

Figure 5 shows the band diagram (in the first Brillouin zone) for the guided modes in TM polarization (H_y). The metallic film has a thickness $L = 256\,nm$. The slits have periodicity $d = 80\,nm$ and width $a = 20\,nm$. The guided band diagram features two distinct types of modes: two surface modes (dotted red curves) and a series of effective dielectric slab modes (solid blue curves). The surface modes are confined to the top and bottom metal-vacuum interfaces, respectively. They are degenerate and have the characteristics of surface plasmon modes on a flat surface. At low frequency, the surface modes asymptotically approach the light line in the ambient environment. The band approaches $\omega = 0.332 \cdot 2\pi c/d$ at the Brillouin zone edge. At large values of the propagation constant k_x , in an extended Brillouin zone representation, we expect the frequency of the surface modes to approach the surface plasmon frequency $\omega_p/\sqrt{2}$ of the metal-vacuum interface. However, in this system it becomes difficult to distinguish between the surface modes and the effective dielectric slab modes above $\omega = 0.332 \cdot 2\pi c/d$. The slits in the plasmonic film, regardless of how narrow they are, always support a propagating state. This state gives rise to a series of effective dielectric slab modes. These modes derive their name from the fact that a similar perfect electric conductor (PEC) system has been shown to be equivalent to a dielectric slab with an effective refractive index.[7] At low frequency, they follow the light line in vacuum. At large k_x , the frequencies approach a series of limiting values, which depend on the order of the mode. While the limiting frequency values are co-determined by geometrical and material parameters, the large- k_x behavior of these modes is quite similar to that of the effective dielectric slab modes found in a PEC system.[7] In the PEC case, the limiting values at large k_x are equally spaced and they are related to the Fabry-Perot resonance condition (section 2.4.). Here, they become increasingly closer to each other as frequency increases.

Figure 6 depicts the field distributions of the modes presented in Fig. 5 for $k_x = 0.50$ (in units of $2\pi/d$). All modes propagate in the x -direction. Shown are the H_y -field distribution of the fundamental effective dielectric slab mode [Fig. 5(a)], the next-higher-order effective dielectric slab mode [Fig. 5(b)], and both degenerate surface modes [Figs. 5(c) and 5(d)]. The surface modes are confined to the lower and upper metal-vacuum interface of the film, respectively. Their field decays rapidly as the distance from the interface increases. The effective dielectric slab modes, on the other hand, have their maximum within the slits of the system and thus indeed resemble the guided modes in a dielectric slab.

Since the system supports two distinct types of guided modes, each with a clear signature for large slab thickness, it is to be expected that these modes will also behave differently when the system parameters are modified. Through careful choice of the geometrical and surface properties, it is possible to control the presence or absence of plasmonic modes and to change their dispersion properties.

Figure 7 shows the dispersion relations when the film thickness L is reduced by a factor of two ($L = 128\,nm, d = 80\,nm, a = 20\,nm$). For the effective dielectric slab modes, this reduction has a profound impact on the behavior at large k_x values: the series of limiting frequency values shift up in a manner which is inversely proportional to L . The thickness of the film affects the Fabry-Perot resonance condition of the electromagnetic state in the slits on which the effective dielectric slab modes rely for their existence.

The surface mode, on the other hand, is almost unaffected by the change in thickness as long as the thickness is large compared to the decay length of the mode inside the slits. The surface modes can be removed if the top and bottom interfaces of the plasmonic film are coated with a thin PEC layer (Fig. 8), since the PEC-vacuum interface does not support a surface mode. The effective dielectric slab modes, on the other hand, remain almost unchanged.

As final remarks, using tabulated data for the dielectric function of silver,[20] we have also analyzed the guided band diagram of this system. For real metal parameters, the main conclusions of the paper, i.e., the existence of two types of guided modes, remain valid. A similar analysis for TE polarization, with electric field parallel to the slits (E_y), revealed that the system does not support any guided modes propagating in the x direction in this polarization. This finding agrees with the results obtained for a perfect metal system.[7]

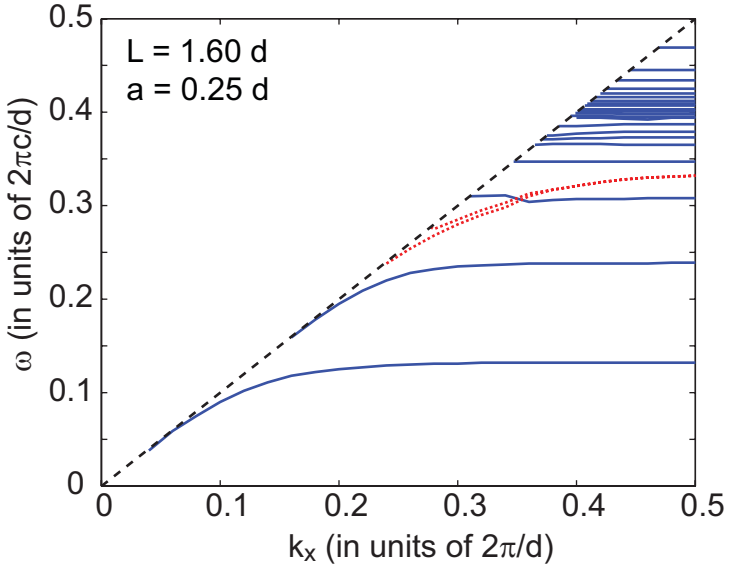

Figure 7: (Color online) Effects of a reduction in film thickness ($L = 128\,nm$, $d = 80\,nm$, $a = 20\,nm$) on the guided-mode band diagram for TM polarization. Shown are two degenerate surface modes (dotted red curves) and a series of effective dielectric slab modes (solid blue curves). The dashed line is the light line in vacuum.

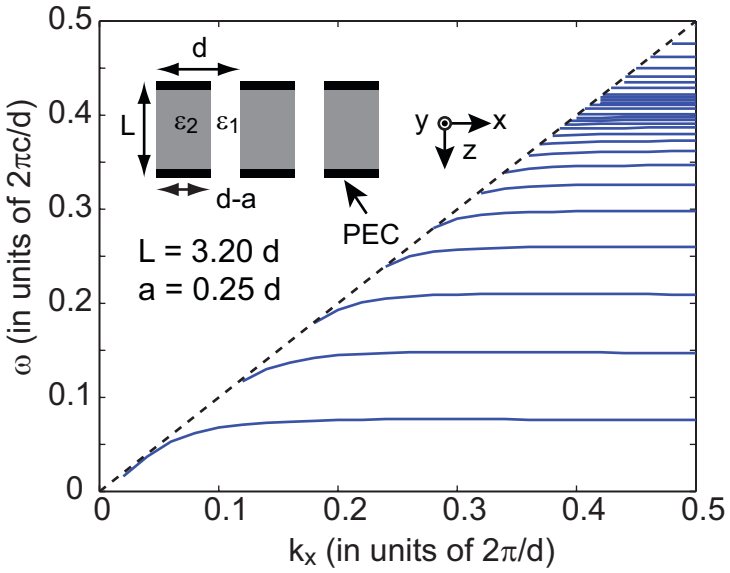

Figure 8: (Color online) Effects of a perfect electric conductor (PEC) coating on plasmonic film on the guided-mode band diagram for TM polarization. Shown are a series of effective dielectric slab modes (solid blue curves); the two degenerate surface modes are not supported. The dashed line is the light line in vacuum. Inset shows the schematic of the metal film with periodic slits. The gray regions indicate metal (ε_2) coated with a thin PEC film (black) and the white regions represent vacuum ($\varepsilon_1 = 1$).

4. CONCLUSION

We presented a mechanism for creating artificial high refractive index metamaterials by exploiting the existence of sub-wavelength propagating modes in metallic systems. We showed that a perfect metal film with a periodic arrangement of sub-wavelength cut-through slits can be regarded as a dielectric slab with a frequency-independent effective index. Next, we analyzed the optical properties of such a system when the perfect metal condition is no longer valid, e.g., in the visible and near infrared wavelength regimes. If the metal obeys a plasmonic dispersion model, we found that this system supports two distinct types of guided modes: a surface mode and a set of effective dielectric slab modes. We discussed how the behavior of both modes is affected by film thickness and surface properties.

ACKNOWLEDGMENTS

This work is supported in part by National Science Foundation Grant No. ECS-0134607 and by Air Force Office of Scientific Research Grant No. FA9550-04-1-0437.

REFERENCES

1 D. Sievenpiper, L. J. Zhang, R. F. J. Broas, N. G. Alexopolous, and E. Yablonovitch, "High-impedance electromagnetic surfaces with a forbidden frequency band," IEEE Trans. Microw. Theory Tech. **47** (11), 2059-2074 (1999).
2 D. R. Smith and N. Kroll, "Negative refractive index in left-handed materials," Phys. Rev. Lett. **85** (14), 2933-2936 (2000).
3 J. B. Pendry, A. J. Holden, D. J. Robbins, and W. J. Stewart, "Magnetism from conductors and enhanced nonlinear phenomena," IEEE Trans. Microw. Theory Tech. **47** (11), 2075-2084 (1999).
4 J. B. Pendry, L. Martin-Moreno, and F. J. Garcia-Vidal, "Mimicking surface plasmons with structured surfaces," Science **305** (5685), 847-848 (2004).
5 B. T. Schwartz and R. Piestun, "Total external reflection from metamaterials with ultralow refractive index," J. Opt. Soc. Am. B: Opt. Phys. **20** (12), 2448-2453 (2003).
6 J. B. Pendry, A. J. Holden, W. J. Stewart, and I. Youngs, "Extremely low frequency plasmons in metallic mesostructures," Phys. Rev. Lett. **76** (25), 4773-4776 (1996).
7 Jung-Tsung Shen, Peter B. Catrysse, and Shanhui H. Fan, "Mechanism for designing metallic metamaterials with a high index of refraction," Phys. Rev. Lett. **94**, 197401 (2005).
8 J. T. Shen and P. M. Platzman, "Properties of a one-dimensional metallophotonic crystal," Phys. Rev. B: Condens. Matter **70** (3), 035101 (2004).
9 P. Lalanne, J. P. Hugonin, S. Astilean, M. Palamaru, and K. D. Moller, "One-mode model and Airy-like formulae for one-dimensional metallic gratings," J. of Opt. A: Pure Appl. Opt. **2** (1), 48-51 (2000).
10 J. A. Porto, F. J. Garcia-Vidal, and J. B. Pendry, "Transmission resonances on metallic gratings with very narrow slits," Phys. Rev. Lett. **83** (14), 2845-2848 (1999).
11 H. Shin, M. F. Yanik, S. H. Fan, R. Zia, and M. L. Brongersma, "Omnidirectional resonance in a metal-dielectric-metal geometry," Appl. Phys. Lett. **84** (22), 4421-4423 (2004).
12 T. W. Ebbesen, H. J. Lezec, H. F. Ghaemi, T. Thio, and P. A. Wolff, "Extraordinary optical transmission through sub-wavelength hole arrays," Nature **391** (6668), 667-669 (1998).
13 E. N. Economou, "Surface plasmons in thin films," Physical Review **182** (2), 539 (1969).
14 Y. Takakura, "Optical resonance in a narrow slit in a thick metallic screen," Phys. Rev. Lett. **86** (24), 5601-5603 (2001).
15 G. Veronis, R. W. Dutton, and S. H. Fan, "Method for sensitivity analysis of photonic crystal devices," Opt. Lett. **29** (19), 2288-2290 (2004).
16 S. D. Wu and E. N. Glytsis, "Finite-number-of-periods holographic gratings with finite-width incident beams: analysis using the finite-difference frequency-domain method," J. Opt. Soc. Am. A **19** (10), 2018-2029 (2002).

17 S. H. Fan, P. R. Villeneuve, and J. D. Joannopoulos, "Large omnidirectional band gaps in metallodielectric photonic crystals," Phys. Rev. B: Condens. Matter **54** (16), 11245-11251 (1996).
18 Jian-Ming Jin, *The Finite Element Method in Electromagnetics*, 2nd ed. (Wiley, New York, 2002).
19 H. van der Lem, A. Tip, and A. Moroz, "Band structure of absorptive two-dimensional photonic crystals," J. Opt. Soc. Am. B: Opt. Phys. **20** (6), 1334-1341 (2003).
20 Edward D. Palik, *Handbook of Optical Constants of Solids*. (Academic Press, Orlando, 1985).